

THE ROLE OF AlGaN BUFFERS AND CHANNEL THICKNESS IN THE ELECTRONIC TRANSPORT PROPERTIES OF $\text{Al}_x\text{In}_{1-x}\text{N}/\text{AlN}/\text{GaN}$ HETEROSTRUCTURES

*M. Amirabbasi**

*Department of Physics, Independent Research Center
Shahrood, Iran*

Received June 24, 2015

We try to theoretically analyze the reported experimental data of the $\text{Al}_x\text{In}_{1-x}\text{N}/\text{AlN}/\text{GaN}$ heterostructures grown by MOCVD and quantitatively investigate the effects of AlGaN buffers and the GaN-channel thickness on the electrical transport properties of these systems. Also, we obtain the most important effective parameters of the temperature-dependent mobility in the range 35–300 K. Our results show that inserting a 1.1 μm thick $\text{Al}_{0.04}\text{Ga}_{0.96}\text{N}$ buffer enhances electron mobility by decreasing the effect of phonons, the interface roughness, and dislocation and crystal defect scattering mechanisms. Also, as the channel thickness increases from 20 nm to 40 nm, the electron mobility increases from 2200 to 2540 $\text{cm}^2/\text{V}\cdot\text{s}$ and from 870 to 1000 $\text{cm}^2/\text{V}\cdot\text{s}$ at 35 and 300 K respectively, which is attributed to the reduction in the dislocation density and the strain-induced field. Finally, the reported experimental data show that inserting a 450 nm graded AlGaN layer before an $\text{Al}_{0.04}\text{Ga}_{0.96}\text{N}$ buffer causes a decrease in the electron mobility, which is attributed to the enhancement of the lateral size of roughness, the dislocation density, and the strain-induced field in this sample.

DOI: 10.7868/S004445101601017X

1. INTRODUCTION

III-nitride compounds and their alloys such as AlGaN and InAlN have received much attention specially in nitride-based high-electron-mobility transistors (HEMTs) because of their fundamental physical properties such as a large band gap, a large breakdown field, and strong spontaneous and piezoelectric polarization fields [1]. Improving the performance of nitride-based HEMTs by increasing the sheet carrier density and carrier mobility in the active channel was a crucial problem for several years. Kuzmik proposed to use nearly lattice-matched InAlN/GaN to improve the two-dimensional electron gas (2DEG) transport properties of nitride-based HEMTs [2, 3]. The advantage of using an AlInN barrier is in adjusting the composition of the alloys to obtain a lattice or polarization-matched structure [4]. For high-power and high-frequency transistors operations, the conductivity performance of the InAlN-based devices should be improved by controlling the effective scattering mechanisms of carrier mobility by choosing the optimized

growth technique. Therefore, the growth of AlInN is still a crucial problem and the number of reports on AlInN and AlInN/GaN heterostructures in the literature is rapidly increasing [4–9]. In [7], the mobility was improved to 5308 $\text{cm}^2/\text{V}\cdot\text{s}$ and 1425 $\text{cm}^2/\text{V}\cdot\text{s}$ at 77 K and room temperature respectively by inserting a 1.2 nm thick AlN interlayer between AlInN and GaN layers.

Transport properties such as the carrier mobility (μ) and the sheet carrier concentration (n_s) are essentially important because operation of all HEMTs devices depends critically on current transport. Therefore, we here try to theoretically analyze the reported experimental data on the $\text{Al}_x\text{In}_{1-x}\text{N}/\text{AlN}/\text{GaN}$ heterostructures grown by MOCVD and investigate the effects of AlGaN buffers and the GaN-channel thickness on the electrical transport properties of these systems, reported in [8], by using simple analytic expressions for scattering mechanisms such as the interface roughness (IFR), alloy disorder, ionized impurity scattering due to the interface charge and remote donors, deformation-potential acoustic phonon scattering, piezoelectric scattering, polar-optical phonon scattering, and crystal defects, which govern transport properties in the temperature range 35–300 K.

* E-mail: mo.amirabbasi@gmail.com

InAlN barrier layers were grown on c-plane sapphire in a low-pressure metal–organic chemical vapor deposition system [8]. Other experimental details are given in Ref. [8]. Sample A, $\text{Al}_{0.82}\text{In}_{0.18}\text{N}/\text{AlN}/\text{GaN}$, is a control sample, and in samples B and C, $\text{Al}_{0.82}\text{In}_{0.18}\text{N}/\text{AlN}/\text{GaN}/\text{Al}_{0.04}\text{Ga}_{0.96}\text{N}$, a 1.1 μm $\text{Al}_{0.04}\text{Ga}_{0.96}\text{N}$ buffer layer is inserted and the thickness of GaN channel is 20 nm and 40 nm for respective samples B and C. In sample D, $\text{Al}_{0.82}\text{In}_{0.18}\text{N}/\text{AlN}/\text{GaN}/\text{Al}_{0.04}\text{Ga}_{0.96}\text{N}/\text{Al}_x\text{Ga}_{1-x}\text{N}$, a 450 nm graded $\text{Al}_x\text{Ga}_{1-x}\text{N}$ layer ($x = x_1, x_2$) was deposited by linearly lowering the Al composition x from $x_1 = 100\%$ to $x_2 = 4\%$ [8]. The cross-sectional schematic diagrams of the investigated AlInN heterostructures are shown in Ref. [8] (see Fig. 1 in Ref. [8]). Also, the sheet carrier concentration of the 2DEG in respective samples A–D have been reported as $2.54 \cdot 10^{13}$, $2.05 \cdot 10^{13}$, $1.95 \cdot 10^{13}$, and $1.79 \cdot 10^{13} \text{ cm}^{-2}$ [8].

2. THEORY OF SCATTERING MECHANISMS

Different scattering mechanisms have been considered to evaluate the mobility. The final value has been obtained using the Matthiessen's rule $1/\mu = \sum_i 1/\mu_i$, where μ_i is the contribution due to the i th scattering mechanism, which is calculated independently. The material parameters used in the calculations are listed in Table 1. We briefly summarize the scattering mechanisms formulas below.

2.1. Intrinsic scattering mechanisms

(I) The polar optical phonon scattering, which controls carrier mobility at high temperatures, is expressed as [15]

$$\mu_{pop}(T) = \frac{4\pi\epsilon_0\epsilon_p\hbar^2}{e\omega(m^*)^2L} \left[\exp\left(\frac{\hbar\omega}{k_B T}\right) - 1 \right], \quad (1)$$

where $L = 2(n_s/10^{12} \text{ cm}^{-2})^{-1/3} \cdot 55 \text{ \AA}$ [16] is the width of the quantum well, n_s is the 2DEG sheet carrier density, and

$$1/\epsilon_p = 1/\epsilon_\infty - 1/\epsilon_s. \quad (2)$$

(II) The acoustic deformation potential scattering is given by [17]

$$\mu_{ac}(T) = \frac{e\hbar^3 \rho u_l^2 L}{m^{*2} E_l^2 k_B T}, \quad (3)$$

where u_l is the longitudinal acoustic phonon velocity.

(III) In strongly polar materials, the most powerful interaction with acoustic phonons at low energies is via

the piezoelectric effect. The piezoelectric scattering is expressed as [18]

$$\mu_{pz}(T) = \frac{\pi k_f E_l^2}{L e^2 \hbar_{14}^2} \times \left[\frac{9}{32} + \frac{13}{32} \left(\frac{u_l}{u_t} \right)^2 \frac{I_A(\gamma_t)}{I_A(\gamma_l)} \right]^{-1} \mu_{dp}, \quad (4)$$

where $k_f = (2\pi n_s)^{1/2}$ is the wave vector on the Fermi surface, \hbar_{14} is the piezoelectric constant, u_t is the transverse acoustic phonon velocity, and

$$I_A(\gamma_t) = [(4\gamma_t/3\pi)^2 + 1]^{1/2}, \quad (5)$$

$$I_A(\gamma_l) = [(4\gamma_l/3\pi)^2 + 1]^{1/2}, \quad (6)$$

$$\gamma_t = 2\hbar u_t k_f / k_B T, \quad (7)$$

$$\gamma_l = 2\hbar u_l k_f / k_B T. \quad (8)$$

2.2. Extrinsic scattering mechanisms

(I) In heterostructures with a 2DEG, although free electrons are separated from the ionized donors, they can still scatter from them. Mobility caused by the ionized impurity scattering due to remote donors scattering [16] is

$$\mu_{remote}(T) = \frac{64\pi\hbar^3 k_f^3 \epsilon_0^2 \epsilon_s^2 S_0^2}{e^3 (m^*)^2 N_d} \times \left(\frac{1}{L_0^2} - \frac{1}{LM_0^2} \right)^{-1}, \quad (9)$$

where

$$L_0 = d_0 + L/2, \quad (10)$$

$$LM_0 = L_0 + d_1, \quad (11)$$

d_0 is the width of the spacer layer, d_1 is the width of the depletion layer ($\approx n_s/N_d$, with N_d being the donor density in the barrier), and $S_0 = e^2 m^* / 2\pi\epsilon_0\epsilon_s\hbar^2$ is the screening constant [19].

(II) As mentioned in Ref. [15], in a modulation-doped InAlN/GaN heterostructure, the 2DEG is formed on the GaN side of the InAlN heterointerface and hence the background impurity scatters free carriers, as does the interface charge. The formula of ionized impurity scattering due to interface charges is [20,21]

$$\mu_{bi} = \frac{4\pi\epsilon_0^2 \epsilon_s^2 \hbar^3 k_f^3}{e^3 (m^*)^2 N_{bi} I_B}, \quad (12)$$

where N_{bi} is the 2D impurity density in the potential well due to background impurities and/or the interface charge and

Table 1. Values of InN material parameters used in the scattering formulas

Material parameters	Values
Density of the crystal ρ [10]	$6.81 \cdot 10^3 \text{ kg/m}^3$
Deformation potential energy E_l [11]	7.10 eV
High-frequency dielectric constant ε_∞ [12]	$8.4\varepsilon_0 \text{ Fm}^{-1}$
Static dielectric constant ε_s [10]	$15\varepsilon_0 \text{ Fm}^{-1}$
Effective mass m^* [12]	$0.14m_0 \text{ kg}$
InN lattice constant [12]	$c = 0.57 \text{ nm}$ $a = 0.353 \text{ nm}$
AlN lattice constant a_l [13]	0.49 nm
The electromechanical coupling coefficient K^2 [14]	0.028

$$I_B = \int_0^\pi \frac{\sin(\varphi)}{[2 \sin(\varphi) + S_0/k_f]^2} d\varphi. \quad (13)$$

(III) The dislocation scattering is expressed as [22, 23]

$$\mu_{disl} = \frac{4\pi\varepsilon_0^2\varepsilon_s^2\hbar^3k_f^4c^2}{e^3(m^*)^2N_{disl}I_t}, \quad (14)$$

where N_{disl} is the charge dislocation density, c is the lattice constant of $(\text{In}_{1-x}\text{Al}_x\text{N})$ it is equal to $xa_l(\text{AlN}) + (1-x)c(\text{InN})$ in accordance with Vegard's law), $\xi = 2kF/qT_F$ is a dimensional parameter, $qT_F = 2/a_B$ is the 2D Thomas–Fermi wave vector, where $a_B = \varepsilon_s\varepsilon_0\hbar^2/\pi e^2m^*$ is the effective Bohr radius in the material, and

$$I_t = 1/2\xi^2 \int_0^1 \frac{1}{(1 + \xi^2u^2)\sqrt{1-u^2}} d\varphi. \quad (15)$$

(IV) In compound (alloy) semiconductors (to which many thermoelectric materials belong), scattering caused by the perturbation of the crystal potential due to the random positioning of substituting atom species in a relevant sublattice is known as alloy disorder scattering. This can only happen in ternary or higher alloys as their crystal structure forms by randomly replacing some atoms in one of the sublattices of the crystal structure.

Mobility caused by the alloy disorder scattering is [24]

$$\mu_{alloy} = \frac{16e\hbar^3}{3bx(1-x)(m^*)^2\Omega^2U_A^2}, \quad (16)$$

where Ω is the volume occupied by one atom, U_A is the alloy potential, x is the Al mole fraction, and

$$b = \left(\frac{33e^2m^*n_s}{8\varepsilon_s\hbar^2} \right)^{1/3} \quad (17)$$

(the Fang–Howard expression).

(V) Surface roughness is a measure of vertical deviations of a surface from a perfectly flat plane. The roughness of interfaces in a heterostructure leads to spatial fluctuations of the potential well width, and consequently to fluctuations of the energy levels. These fluctuations of energy levels act as a fluctuating potential for the motion of confined carriers [25]. As a result, being confined close to the interfaces, the electrons are highly sensitive to irregularities, which can be impurities trapped at the interface or monolayer steps.

The interface roughness scattering is expressed as [26, 27]

$$\mu_{IFR} = \frac{2\varepsilon_s}{n_s\Delta\Lambda} \frac{\hbar^3}{e^3(m^*)^2} \frac{1}{J_{IFR}(k)}, \quad (18)$$

where Δ is the lateral size of the roughness, Λ is the correlation length between fluctuations and

$$J_{IFR}(k) = \int_0^{2k} \frac{\exp(-q^2\Lambda^2/4)}{2k^3(q+q_s)^2\sqrt{1-(q/k)^2}} q^4 dq \quad (19)$$

(a correlation-length and the lateral-size dependent integral),

$$q = 2k \sin(\theta/2) \quad (20)$$

(the reciprocal screening length),

$$q_s = \frac{e^2m^*}{2\pi\varepsilon_s\hbar^2} F(q), \quad (21)$$

and

$$F(q) = b(8b^2 + 9qb + 3q^2)/8(b + q)^3, \quad (22)$$

where θ is the scattering angle.

(VI) Crystal defect scattering is given by [28]

$$\mu_{cd}(T) = \frac{C}{T^{1.5}}, \quad (23)$$

where C is a parameter that is attributed to domain boundaries and strain-induced fields. This mechanism is dominant at high temperatures and Eq. (23) is an experimental relation [28].

2.3. Calculation of transverse and longitudinal acoustic phonon velocity

The acoustic wave in InN consists of two longitudinal and transverse components with the velocities u_l and u_t , which can be obtained from the relations [29]

$$u_l = \sqrt{C_{33}/\rho}, \quad (24)$$

$$u_t = \sqrt{C_{44}/\rho}, \quad (25)$$

where C_{33} and C_{44} are elastic stiffness coefficients, which have been reported as (182 ± 6) GPa and (10 ± 1) GPa, respectively [30].

3. RESULTS AND DISCUSSION

3.1. Band gap

Using Vegard's law and the band gap value of InN (1 eV) [14] and AlN (6.23 eV) [31], we can calculate the band gap value of $\text{In}_{0.18}\text{Al}_{0.82}\text{N}$ to be about 5.28 eV, which means that the band gap of $\text{In}_{0.18}\text{Al}_{0.82}\text{N}$ is wider than that of GaN. We should therefore expect that the part of conduction electrons in the InAlN layer are transferred to an adjacent layer with a smaller band gap (GaN), which causes an internal field and subsequently the formation of a triangular quantum well, and thus the formation of a thin layer near the interface with a 2DEG behavior.

3.2. Temperature-dependent carrier mobility

Experimental data on electron mobility for all samples were given in Ref. [8] (see Fig. 5 in Ref. [8]). It is clear that samples C and D have respective higher and lower electron mobilities.

To analyze these data, we can use different scattering mechanisms (mentioned in Sec. 2) and the related material parameters (see Table 1). Figures A–D and

Table 2 show the computational position of each scattering mechanism and the calculated fitting parameters.

We list the results obtained from Figure as follows.

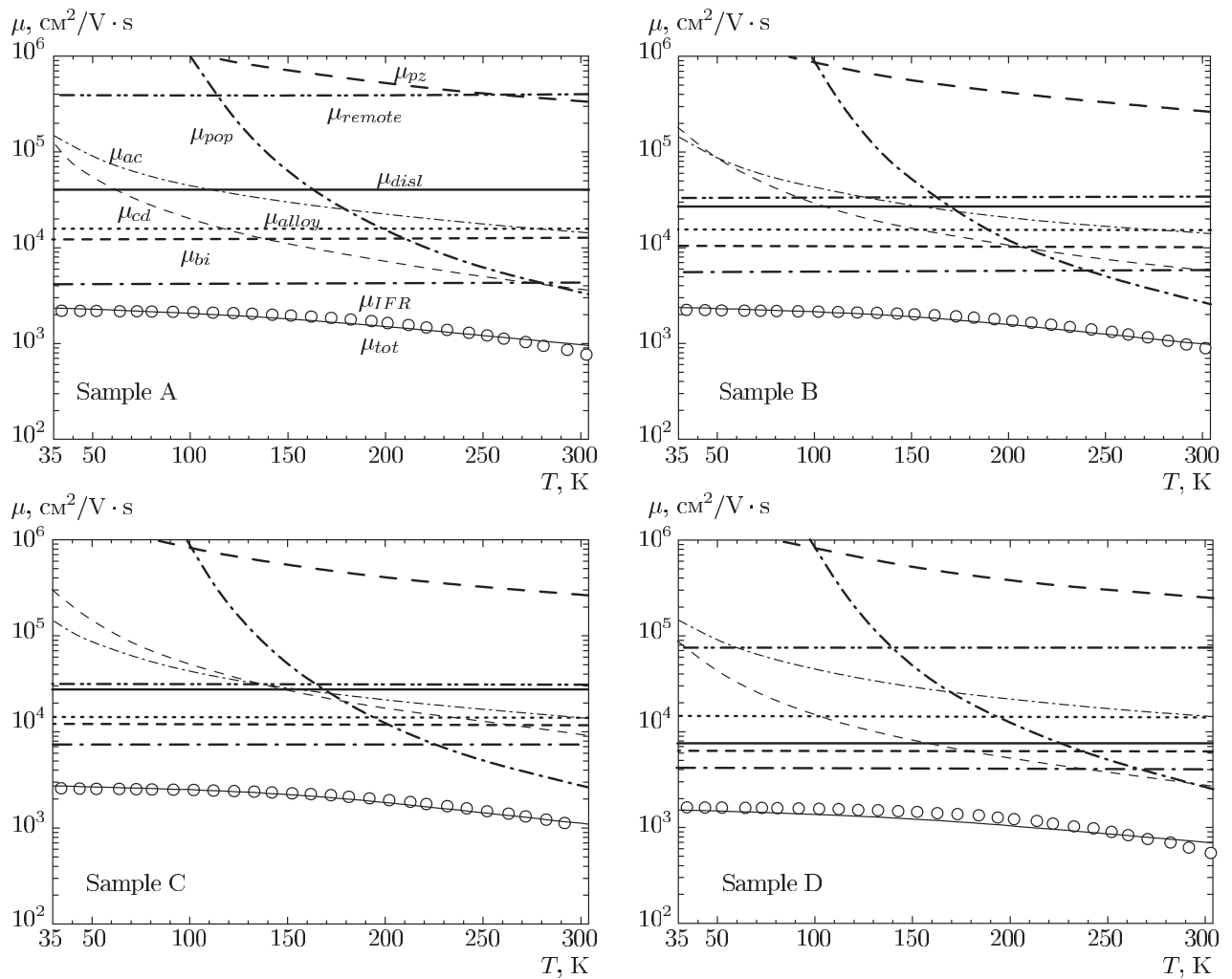
1. For sample A, the dominant mechanism is phonon and crystal defect scattering at high temperatures ($T > 270$ K), and interface roughness scattering at low temperatures ($30 \text{ K} < T < 270 \text{ K}$).
2. For sample B, conductivity is restricted by phonon scattering at high temperatures ($T > 240$ K) and by the interface roughness at low temperatures.
3. For sample C, phonon scattering is dominant at high temperatures ($T > 230$ K) and the interface roughness scattering mechanism is dominant at low temperatures.
4. For sample D, phonon and crystal defect scattering are dominant at high temperatures ($T > 260$ K) and the interface roughness scattering mechanism is dominant at low temperatures.

These results show that the interface roughness scattering mechanism plays an important role in controlling electrical conductivity in AlInN, especially at low temperature. Also, for samples C and D, which have the highest and lowest mobility, phonon scattering is efficient in a wider temperature range ($T > 200$ K) and a narrow temperature range ($T > 260$ K), respectively. We note that the value of the C parameter (see Table 2) and the crystal defect scattering, which is related to strained-induced fields, play a more significant and a less significant role in mobility at high temperature for respective samples C and D. As result, inserting 450 nm thickness AlGaInN decreases the crystalline quality of sample D, because the obtained values of the dislocation density and the 2D impurity density in the potential well for sample D are highest compared with the other samples (see Table 2). As is clear from Sec. 2.1, phonon scattering mechanisms depend on the sheet carrier density via the width of the quantum well and the wave vector on the Fermi surface, and therefore inserting 1.1 μm thick $\text{Al}_{0.04}\text{Ga}_{0.96}\text{N}$ buffers reduces the sheet carrier density which is caused to reduction of phonon scattering especially at high temperatures (samples B and C).

Also, electron mobility increases when the GaN channel thickness changes from 20 nm (sample B) to 40 nm (sample C). This increase can be related to a decrease in the dislocation density, the strained induce field, the ionized impurity density in the well potential, and the lateral size of roughness (see Figure and Table 2). We note that the obtained dislocation density (see Table 2) matches the reported values [32] in the range 10^9 – 10^{11} cm^{-2} .

Table 2. Fitting parameters

Fitting parameters	Sample A	Sample B	Sample C	Sample D
Dislocation density N_{disl}, m^{-2}	$1 \cdot 10^{14}$	$1 \cdot 10^{14}$	$9 \cdot 10^{13}$	$3 \cdot 10^{14}$
2D impurity density in the potential well N_{bi}, m^{-3}	$6 \cdot 10^{24}$	$5 \cdot 10^{24}$	$4 \cdot 10^{24}$	$7 \cdot 10^{24}$
Piezoelectric constant $h_{14}, V/m$	$5.5 \cdot 10^8$			
C Parameter	$2.5 \cdot 10^7$	$3 \cdot 10^7$	$5 \cdot 10^7$	$1.5 \cdot 10^7$
Δ lateral size of the roughness, nm	54	58	51	71
Λ correlation length between fluctuations, Å	2.7	2.5	2.5	2.8



The position of each calculated scattering mechanism in samples A–D. The clues are listed in Fig. A

4. CONCLUSION

We have tried to theoretically analyze the reported experimental data of the $\text{Al}_x\text{In}_{1-x}\text{N}/\text{AlN}/\text{GaN}$ heterostructures grown by MOCVD and to quantitatively investigate the effects of AlGaN buffers and the GaN-channel thickness on the electrical transport properties of these systems. We obtained the most important effective parameters of the temperature-dependent mobility in the range 35–300 K. The obtained results show that with the insertion of $\text{Al}_{0.04}\text{GaN}_{0.96}\text{N}$ buffers, the lateral size of roughness and the dislocation density decrease, which leads to an increase in carrier mobility. For sample D, with insertings graded $\text{Al}_x\text{GaN}_{1-x}\text{N}$ layer, the electron mobility decreased via increasing the effects of interface roughness, dislocation, and crystal defect scattering. Also, as the channel thickness widens from 20 nm to 40 nm, the electron mobility enhances, which is attributed to a reduction in the dislocation density and the strain-induced field.

REFERENCES

1. H. Morkoc, *Handbook of Nitride Semiconductor and Devices*, Wiley-VCH, Berlin (2008), Vols. I–III.
2. J. Kuzmik, *IEE Electron Device Lett.* **22**, 510 (2001).
3. J. Kuzmik, *Semicond. Sci. Technol.* **17**, 540 (2002).
4. R. Tulek, A. Ilgaz, S. Gokden, A. Teke, M. K. Ozturk, M. Kasap, S. Ozcelik, E. Arsalan, and E. Ozbay, *J. Appl. Phys.* **105**, 013707 (2009).
5. A. Koukitu, Y. Kumagai, and H. Seki, *Phys. Stat. Sol. A* **180**, 115 (2000).
6. M. Gonschorek, J. F. Carlin, E. Feltn, and M. A. Py. N. Grandjean, *Appl. Phys. Lett.* **89**, 062106 (2006).
7. J. Xue, J. Zhang, W. Zhang, L. Li, F. Meng, M. Lu, J. Ning, and Y. Hao, *J. Cryst. Growth*, **343**, 110 (2012).
8. O. Kelekci, P. Tasil, S. S. Cetin, M. Kasap, S. Ozcelik, and E. Ozbay, *Current Appl. Phys.* **12**, 1600 (2012).
9. O. Katz, D. Mistele, B. Meyler, and G. Bahir, *J. Salzman IEEE Trans. Electron Devices* **52**, 146 (2005).
10. M. T. L. Tansley, in *Properties of Group III nitrides*, ed. by J. H. Edgar, data reviewers Series N11, an INSPEC publication, 35–40 (1994).
11. S. Gokden, *Chin. J. Phys.* **46**, 145 (2008).
12. H. Harima, *J. Phys.: Cond. Matter.* **14**, R967 (2002).
13. A. Kasic, M. Schubert, Y. Saito, G. Wagner, and Y. Nanishi, *Phys. Rev. B* **65**, 115206/1 (2002).
14. M. Levinshtein, S. Rumyantsev, and M. Shur, *Properties of Advanced Semiconductor Materials: GaN, AlN, InN, BN, SiC, SiGe*, Wiley, Canada (2001).
15. B. K. Ridley, *J. Phys. C* **15**, 5899 (1982).
16. K. Lee, M. S. Shur, T. J. Drummond, and H. Morkoc, *J. Appl. Phys.* **54**, 11 (1983).
17. P. K. Basu and B. R. Nag, *Phys. Rev. B* **22**, 4849 (1980).
18. P. J. Price, *Ann. Phys. NY* **133**, 217 (1981).
19. P. J. Price, *J. Vac. Sci. Technol.* **19**, 599 (1981).
20. K. Hess, *Appl. Phys. Lett.* **35**, 484 (1979).
21. C. T. Sah, T. H. Ning, and L. L. Tscopp, *Surf. Sci.* **32**, 561 (1972).
22. S. Das Sarma and F. Stern, *Phys. Rev. B* **32**, 8442 (1985).
23. J. H. Davies, *The Physics of Low Dimensional Semiconductors*, Cambridge Univ. Press, Cambridge (1998).
24. D. Zanato, S. Gokden, N. Balkan, and W. J. Schaff, *Semicond. Sci. Technol.* **19**, 427 (2004).
25. U. Panner, H. Rucker, and I. N. Yassievich, *Semicond. Sci. Technol.* **13**, 709 (1998).
26. B. K. Ridley, B. E. Foutz, and L. F. Eastman, *Phys. Rev. B* **61**, 16862 (2000).
27. M. J. Kearney and A. L. Horrel, *Semicond. Sci. Technol.* **13**, 174 (1998).
28. H. Tang, W. Kim, A. Botchkarev, G. Popovici, F. Hamdani, and H. Morkoc, *Sol. St. Electr.* **42**, 839 (1998).
29. H. Morkoc and Umit Oagur, *Zinc Oxide Fundamentals, Materials and Device Technology*, WILEY-VCH (2009).
30. I. Vurgaftman, J. R. Meyer, and L. R. Ram-Mohan, *J. Appl. Phys.* **89**, 5815 (2001).
31. A. U. Sheleg and V. A. Savastenko, *Izv. Akad. Nauk SSSR. Neorg. Mater.* **15**, 1598 (1979).
32. C. S. Gallinat, G. Koblmuller, F. Wu, and J. S. Speck, *J. Appl. Phys.* **107**, 053517 (2010).